Materials Research Proceedings 28 (2023) 357-366 https://doi.org/10.21741/9781644902479-39

Modeling multiaxial stress states in forming simulation of woven fabrics

KÄRGER Luise[1,a *], SCHÄFER Florian[1,b] and WERNER Henrik O.[1,2,c]

[1] Karlsruhe Institute of Technology (KIT), Institute of Vehicle System Technology, Institute Division Lightweight Design, Karlsruhe, Germany

[2] Karlsruhe Institute of Technology (KIT), Institute of Applied Materials, Institute Division Material Sciences, Karlsruhe, Germany

[a]luise.kaerger@kit.edu, [b] florian.schaefer93@t-online.de, [c] henrik.werner@kit.edu

Keywords: Hyperelastic, Invariant-Based, Constitutive Modeling, Multiaxial Coupling

Abstract. During the forming of woven fabrics, different multiaxial stress states can occur, depending on the given process conditions and the complex deformation mechanisms of the interwoven structure of the textile. Particularly under constrained forming conditions, induced e.g. by blank holders or by adjacent metal layers in fiber-metal-laminate (FML) forming, the multiaxial stress states may include in-plane compression. A hyperelastic, invariant-based constitutive model has been proposed in previous work to consider such biaxial and normal-shear coupling for both positive and also negative strains. In the present work, this constitutive model is applied to forming simulation at component scale to investigate the significance of individual coupling aspects for the prediction of the forming behavior under different multiaxial stress states. For that purpose, FMLs and pure fabric laminates are formed to a tetrahedron geometry. In a comparative simulation study, the individual strain couplings of the invariant-based material model are differently activated or suppressed. The simulation results reveal that biaxial coupling has a significant effect on the draping behavior, if the draping is partially constrained. In contrast, the coupling effects are much smaller for free draping conditions.

Introduction

In the past two decades, a large number of material models have been developed to describe the forming behavior of textile materials at meso and macro scale [1,2]. However, only macroscale models are suitable for forming simulation at component level [3] and enable virtual validation and optimization of forming processes [4,5]. Since textiles are prone to large shear, non-orthogonal material models are required [6-8]. This can be realized by hypoelastic or hyperelastic material modeling. Hypoelastic approaches [9-11] describe stress rates as direct functions of strain rates, depending on the stiffness. At each timestep, stress increments can be calculated directly from strain increments, which makes hypoelastic approaches convenient for implementation in nonlinear finite element approaches. For sufficient accuracy, however, they require sufficiently small timesteps. The advantage of hyperelastic approaches [12-14] is the integral representation of the stress-strain relationship, which enables timestep-independent solutions. The stress-strain relation is based on the strain energy density and their differentiation with respect to strain measures.

For woven fabrics that exhibit pronounced orthotropy with two preferred directions, the strain energy potential can be easily decomposed into distinct strain energy components, depending on different invariants of the deformation state [15-17]. The invariant-based energy formulation has the additional advantage of being independent of the choice of the basis reference system. Since experimental studies have shown interdependencies between distinct strain components, hyperelastic models with invariant-coupling, e.g., biaxial-tension [18] and tension-shear coupling

[19], have been proposed. A recent review on modelling coupling mechanisms in woven fabrics, with particular focus on invariant-based constitutive modeling is given in [20].

In the context of fiber-metal-laminate (FML) forming, Schäfer et al. [21] have introduced an invariant-based model, which considers both biaxial and normal-shear coupling, but not just for positive strains (i.e. tension), but also for negative strains. The additional consideration of compressive strains in biaxial and normal-shear coupling becomes necessary, if wrinkling is suppressed during forming, e.g. due to adjacent metal layers as in FML forming, but also due to blank holders or grippers [21]. Under such constrained condition in thickness direction, the bending and wrinkling behavior becomes insignificant compared to the complexly interacting components of the membrane behavior, namely shear, tension and compression [22,23].

In the present work, the invariant-based constitutive model presented by Schäfer et al. [21] is used to evaluate the significance of different strain couplings in forming simulation at component scale. For that purpose, the invariants that control the couplings in the different components of the strain energy densities are activated or suppressed in different combinations. Additionally, the effects are compared for strongly constrained forming of FML and less constrained forming of a pure fabric laminate. First, the material [21] is summarized with the most essential equations to indicate the interactions that are considered in the strain energy density components. Subsequently, the numerical test case, a tetrahedron geometry, and the applied materials are introduced. Finally, the forming simulation results are presented and discussed in terms of the coupling aspects and their significance on the forming results for varying forming conditions.

Hyperelastic Multiaxially Coupled Invariant-Based Constitutive Model

The hyperelastic invariant-based model, examined in this work for multiaxial coupling effects, was originally proposed and verified in our previous work [21]. For the sake of brevity, only the most important equations of the model are presented in the following. For more details, the reader is kindly referred to [21]. The invariant-based model was implemented in a user subroutine VUMAT for forming simulation in ABAQUS/EXPLICIT. Membrane and bending behavior are modeled in a decoupled way by superimposed finite membrane elements M3D3 and finite shell elements S3R. The membrane elements use the new VUMAT, while the shell elements use a bending idealization with section integration and deactivated membrane properties.

The basic assumption of the membrane model is the additive decomposition of the total strain energy density

$$W_{tot} = W_{TC}(I_4, I_8) + W_{S,TC}(I_{10}, I_4, I_8) \tag{1}$$

into a tension-compression component $W_{TC}(I_4, I_8)$ and a tension-compression-dependent shear component $W_{S,TC}(I_{10}, I_4, I_8)$. The components are based on invariants I_i of the right Cauchy-Green (RCG) tensor to be independent of the choice of the coordinate system.

Tension-compression coupling.

The tension-compression-dependent strain energy density component W_{TC} is composed of two components $W_{M,a}$ and $W_{N,b}$ according to the two fiber directions a and b, where the indices M and N represent tension (T) or compression (C). The composition depends on the current strain state:

$$W_{TC}(I_4, I_8) = W_{M,a}(I_4, I_8) + W_{N,b}(I_4, I_8) \tag{2}$$

with $M = T$ for $I_4 > 1$; $M = C$ for $I_4 \leq 1$; $N = T$ for $I_8 > 1$; and $N = C$ for $I_8 \leq 1$ [21]. The invariants I_4 and I_8 are the quadratic stretches in fiber directions a and b, respectively.

For tension, the strain energy densities are

$$W_{T,a}(I_4, I_8) = \widehat{W}_{T,a}(I_4) \cdot k_{TC,a}(I_8) \quad and \quad W_{T,b}(I_4, I_8) = \widehat{W}_{T,b}(I_8) \cdot k_{TC,b}(I_4) \tag{3}$$

with the uniaxial strain energy densities

$$\widehat{W}_{T,a} = a_a\left(\sqrt{I_4} - 1\right)^3 + b_a\left(\sqrt{I_4} - 1\right)^2; \quad \widehat{W}_{T,b} = a_b\left(\sqrt{I_8} - 1\right)^3 + b_b\left(\sqrt{I_8} - 1\right)^2 \tag{4}$$

where a_i and b_i are material parameters to be determined by unidirectional tensile tests. In Eq. (3), the influence of transverse strains is considered by the fiber-fiber-interaction factors

$$k_{TC,a}(I_8) = exp\ exp\ \left(c_a\left(\sqrt{I_8}-1\right)\right) + p_{min,a}\ \left(1 - exp\ exp\ \left(c_a\left(\sqrt{I_8}-1\right)\right)\right) \quad (5)$$

$$k_{TC,b}(I_4) = exp\ exp\ \left(c_b\left(\sqrt{I_4}-1\right)\right) + p_{min,b}\ \left(1 - exp\ exp\ \left(c_b\left(\sqrt{I_8}-1\right)\right)\right) \quad (6)$$

taking values greater than 1 for transverse tension and values between 0 and 1 for transverse compression. The tension-compression parameter $p_{min,i}$ is introduced to limit the influence of the transverse strains on the tensile strain energy density, which is particular important in the case of negative transverse strains [21]. $p_{min,i}$ can take values between 0 (complete strain energy reduction due to compression is possible) and 1 (no influence). In this work, $p_{min,i}$ is set to 0.75 for negative and positive transverse strains. Primarily, the biaxial coupling coefficient c_i provides a strictly monotonous increase or decrease of the strain energy density for positive or negative transverse strains, respectively. It can be determined by biaxial tension tests.

Compression is typically not considered in composite forming simulation, since the textile material can easily buckle and wrinkling can occur. However, under constrained conditions, e.g. by blank holders or adjacent metal layers, wrinkling is suppressed and the resulting multiaxial stress states may include in-plane compression. In this case, a linear stress-strain relation and no strain components coupling is assumed, leading to the compressive strain energy densities

$$W_{C,a}(I_4) = d_a\left(\sqrt{I_4}-1\right)^2 \qquad and \qquad W_{C,b}(I_8) = d_b\left(\sqrt{I_8}-1\right)^2 \quad (7)$$

where d_i are material parameters that are proportional to the compressive [21]. To date, there is no test setup available for a reliable characterization of the compressive stiffness, since the fabrics are prone to buckling. Therefore, the compression stiffness is assumed according to numerical parameter studies performed by Werner et al. [23].

Normal-shear coupling.

Shear is a prevalent deformation mechanism in woven fabrics, and thus, crucial for material modeling. According to the mesoscopic nature of the interwoven fiber bundles, pure shear can be divided in three zones with very low, medium and high shear stiffness. To capture this steadily increasing shear stiffness, a polynomial of third order is assumed for the stress-strain relation, which leads to the shear strain energy density

$$W_S(I_{10}) = \frac{1}{2}s_1 I_{10}^2 + \frac{1}{3}s_2 I_{10}^3 + \frac{1}{4}s_3 I_{10}^4 \quad (8)$$

where the shear invariant I_{10} represents the shear angle, and material parameters s_i can be determined by pure shear tests [21]. The shear strain energy density is increased for superimposed fiber tension and decreased for superimposed fiber compression. In the case of positive fiber strains, additional strain energy densities

$$W_{ST,a}(I_{10}, I_4) = \frac{1}{3}\ I_{10}^3\ s_{T,a}\ (I_4 - 1)^2\ ; \quad W_{ST,b}(I_{10}, I_8) = \frac{1}{3}\ I_{10}^3\ s_{T,b}\ (I_8 - 1)^2 \quad (9)$$

are added, where $s_{T,i}$ are material parameters that can be determined by combined tension-shear tests [21]. In the case of negative fiber strains, the shear strain energy densities (8) and possibly (9) are multiplied by exponential reduction factors

$$k_{SC,a}(I_4) = exp\ exp\left(s_{C,a}(I_4 - 1)^3\right); \qquad k_{SC,b}(I_8) = exp\ exp\left(s_{C,b}(I_8 - 1)^3\right) \quad (10)$$

with the compression-shear parameter $s_{C,a}$ to achieve a smooth asymptotic reduction of the shear strain energy density [21]. Thus, $k_{SC,i}$ can take values less or equal to 1, but always greater than zero.

Total strain energy density.

Combining the tension strain energy density (3) and the compression strain energy (7) with the shear strain energy density (8), influenced by fiber tension (9) or fiber compression (10), yields:

$$W_{\mathrm{tot}} = \begin{cases} W_{\mathrm{T,a}} + W_{\mathrm{T,b}} + W_{\mathrm{S}} + W_{\mathrm{ST,a}} + W_{\mathrm{ST,a}} & \text{for} \quad I_4 > 1 \text{ and } I_8 > 1 \\ W_{\mathrm{T,a}} + W_{\mathrm{C,b}} + \left(W_{\mathrm{S}} + W_{\mathrm{ST,a}}\right) \cdot \ k_{\mathrm{SC,b}} & \text{for} \quad I_4 > 1 \text{ and } I_8 \leq 1 \\ W_{\mathrm{C,a}} + W_{\mathrm{T,b}} + \left(W_{\mathrm{S}} + W_{\mathrm{ST,b}}\right) \cdot \ k_{\mathrm{SC,a}} & \text{for} \quad I_4 \leq 1 \text{ and } I_8 > 1 \\ W_{\mathrm{C,a}} + W_{\mathrm{C,b}} + W_{\mathrm{S}} \cdot \ k_{\mathrm{SC,a}} \cdot \ k_{\mathrm{SC,b}} & \text{for} \quad I_4 \leq 1 \text{ and } I_8 \leq 1 \end{cases} \tag{11}$$

Fig. 1 depicts total strain energy surfaces for selected shear angles I_{10}.

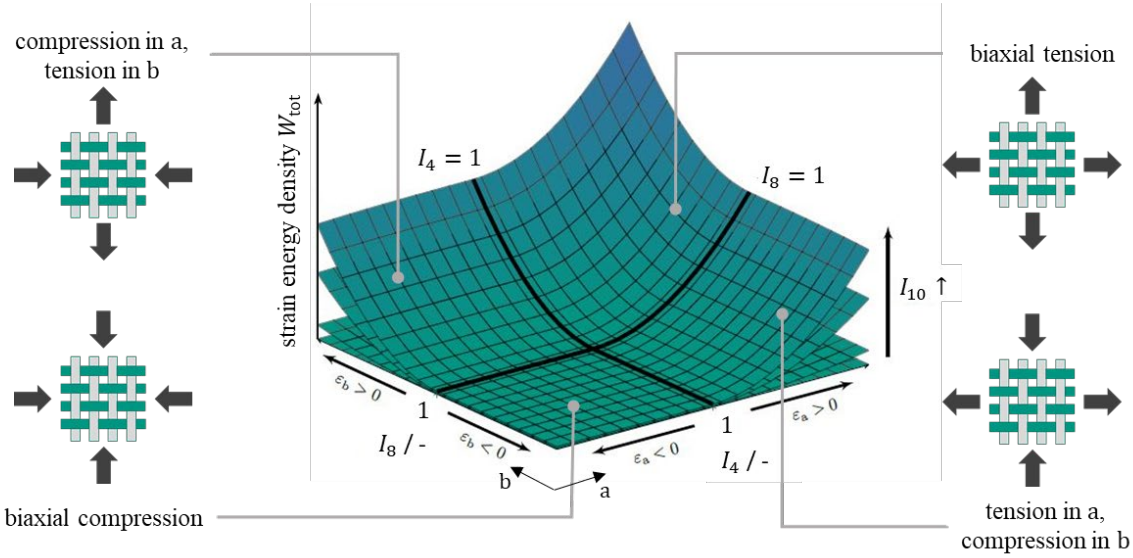

Fig. 1. Qualitative representation of the total strain energy density W_{tot} for selected shear angles I_{10} and with dependence on the invariants I_4 and I_8. The bold lines $I_4 = 1$ and $I_8 = 1$ represent superposition of uniaxial load in fiber directions b and a, respectively, with shear I_{10} [21].

Model verification.

The prediction capability of the new multiaxially-coupled invariant-based constitutive model was verified by means of tensile and bias-extension tests [21], partly with comparison to experimental results. The simulation results of these verification tests at coupon level revealed that the new model is capable to capture transverse coupling effects, i.e. transverse stresses in the case of constrained loading and, vice versa, transverse strains in the case of free loading [21]. This is in contrast to the ABAQUS built-in FABRIC model, which is not able to predict transverse effects. In Fig. 2, the effect of differently activated coupling mechanisms is illustrated at the example of a simple uniaxial tensile test, where the resulting transverse strain component ε_{22} is compared to experimental results from Cherouat and Bourouchaki [24]. The results in Fig. 2 and particularly in Fig. 2 (b) confirm that the biaxial normal strain coupling is responsible for correctly predicting the deformed fabric shape [21], which is clearly concave in transverse direction, as observed in experiments [24].

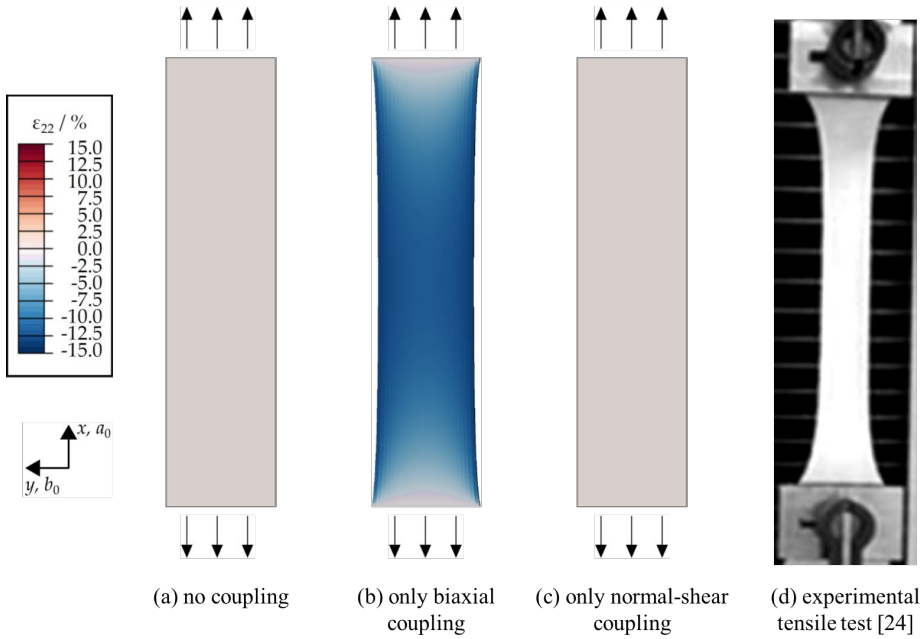

Fig. 2. Transverse strain component ε_{22} in a uniaxial tensile test for differently activated couplings [21].

Parametric Study on Individual Multiaxial Couplings and their Effects on Forming Results

To investigate the significance of the different tension-compression and normal-shear interactions, the proposed constitutive model is applied to forming simulation at component scale. Furthermore, forming simulation of a fiber-metal laminate (FML) is compared to forming simulation of a pure fabric to analyze the effect of different forming constraints on the multiaxial interactions.

Numerical test case and materials.

A 280 x 280 mm FML with three woven fabric layers and two metallic cover layers is formed into a tetrahedron shape, following the work of Yao et al. [19]. For comparison, three fabric layers without metal blanks are formed into the same geometry. In both cases, a blank holder pressure of 2 MPa is applied to prevent wrinkling. The inter-ply behavior between the rigid-body tools, the metal sheets and the fabric plies is modelled as COULOMB friction with the same friction parameters as used in [21]. The model setup including dimensions and boundary conditions is given in Fig. 3.

The metal material is steel DC04 and is assumed to behave elastic-plastic, as characterized experimentally and modelled by Werner et al [22,23].The fabric material is a plain weave fabric according to the industrial TWINTEX® TPP60N22P-060 with comingled glass/PP fibers, used and characterized by Komeili et al. [25]. The material behavior of the woven fabric is assumed nonlinear elastic according to the equations given in Section 2. The material parameters of the nonlinear models for steel and woven fabric are all the same as in our previous work [21], partly taken from the mentioned literature [22,23,25] and partly assumed. Failure and damage are not considered, neither in the metal sheets nor in the woven fabric.

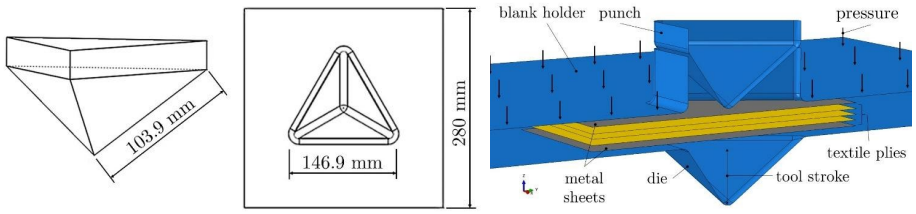

Fig. 3. Tetrahedron geometry: Dimensions and half FE-model of tool and FML.

Materials Research Proceedings 28 (2023) 357-366 https://doi.org/10.21741/9781644902479-39

It needs to be noted that the forming simulation example is a purely numerical test case to expose the effect of different interactions. Some of the material parameters are assumed, the blank holder pressure is comparatively high to avoid wrinkling and the forming simulation is conducted up to a rather large tool stroke with strains reaching values beyond failure or yielding. Nevertheless, the test case is chosen and suited to illustrate the importance of the distinct multiaxial coupling aspects for stronger and weaker forming constraints.

Results for FML forming.

Fig. 4 shows the distribution of the resulting shear angle γ_{12} for the deformed FML, where the Fabric material model available in Abaqus (Fig. 4a) is compared to four different configurations of the new hyperelastic material model with differently activated strain couplings.

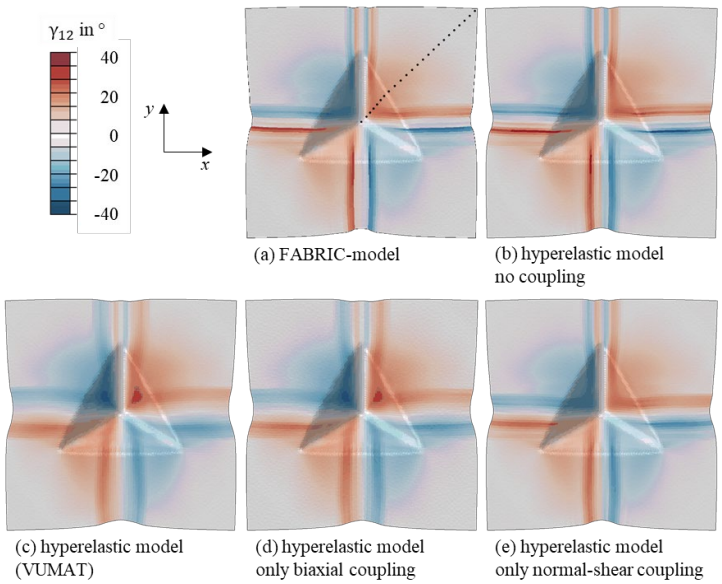

Fig. 4. Shear angles γ_{12} within the inner fabric layers of an FML with two metal blanks, formed into a tetrahedron geometry: Comparison of (a) the FABRIC material model and (b to e) four different configurations of the new hyperelastic material model with differently activated strain couplings.

The results reveal that the *normal-shear coupling* (Fig. 4e) has only marginal effect on the forming results, since the shear angle distribution is comparable to the *FABRIC model* (Fig. 4a) and the *hyperelastic model without coupling* (Fig. 4b). In contrast, the *fully coupled hyperelastic model* (Fig. 4c) and the model with *biaxial normal coupling* (Fig. 4d) lead to considerably higher shear angles. The same conclusion can be drawn from Fig. 5, where the shear angle is plotted along the dotted line in Fig. 4a and is compared for all five configurations. An explanation for the strong influence of *biaxial normal coupling* is the presence of high normal stresses due to the encasing metal layers that hinder formation of wrinkles and promote deformation in shear. Interestingly, just a minor effect of normal-shear coupling can be observed by the green *only normal-shear coupling* curve in Fig. 5. It is located just slightly below the gray *no-coupling* curve, because the higher tensile strains partly impede shear deformation. The same is observed for the *fully coupled VUMAT* model, which is slightly below the *only biaxial coupling* curve that neglects normal-shear coupling.

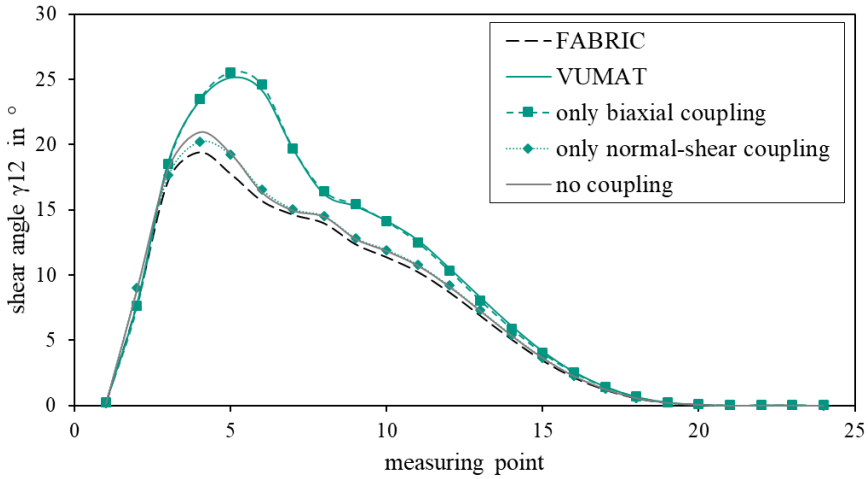

Fig. 5: Shear angle γ_{12} within the formed inner fabric layers of an FML along the dotted line in Fig. 4a: Comparison of the FABRIC material model and four different configurations of the new hyperelastic material model.

Results for pure fabric forming.

To investigate the relevance of biaxial and normal-shear coupling for weakened forming constraints, forming simulations are performed for three fabric layers without metal blanks. Furthermore, the friction coefficient between fabric and tool is smaller than the friction coefficient between fabric and metal sheet, which further reduces the resistance against deformation in the fabric. These modifications are implemented to facilitate shear deformation and material draw-in, and thus, to reduce normal stresses in fiber direction.

The resulting shear angles γ_{12} of the deformed three fabric layers are depicted in Fig. 6. Again, the ABAQUS/EXPLICIT built-in FABRIC model (Fig. 6a) is compared to four configurations of the new hyperelastic material model with differently activated strain couplings. As Fig. 6 reveals, the influence of interacting strain components on the resulting shear deformation is much smaller than in the more strongly constrained FML forming case. This conclusion is again confirmed by Fig. 7, where the shear angle is plotted along the dotted line in Fig. 6a. Again, the results of the fully coupled hyperelastic model (Fig. 6c) and the biaxial normal coupling (Fig. 6d) are close together and are above the results of the other configurations, but the difference between the curves is much smaller than for the constrained forming results shown in Fig. 5. Overall, the shear deformation is, as expected, larger than in the case of FML forming with metal blanks, which results from reduced friction, smaller normal strains and less coupling effects.

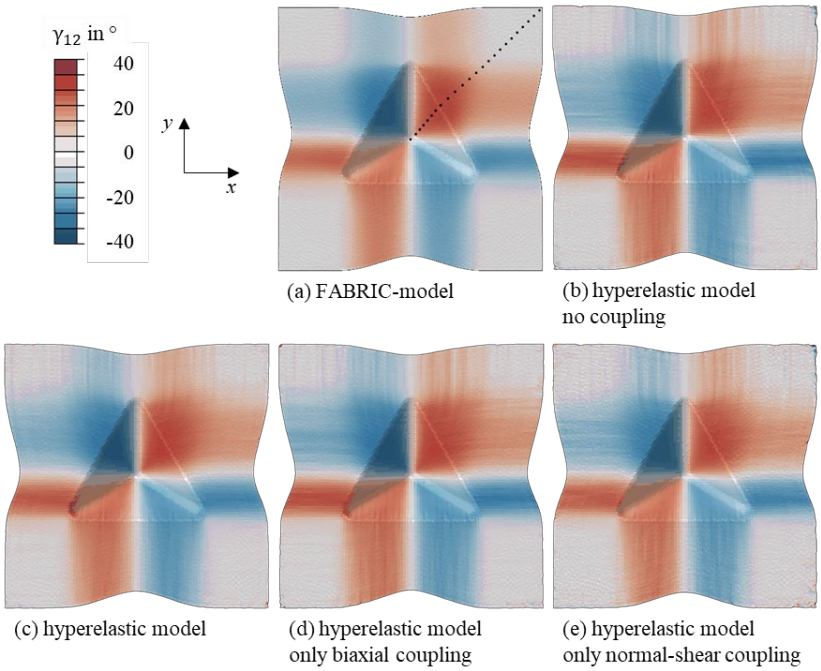

Fig. 6. Shear angle γ_{12} within a pure woven fabric with three fabric layers, formed into a tetrahedron geometry without metal blanks: Comparison of (a) the FABRIC material model and (b to e) four different configurations of the new hyperelastic material model with differently activated strain couplings.

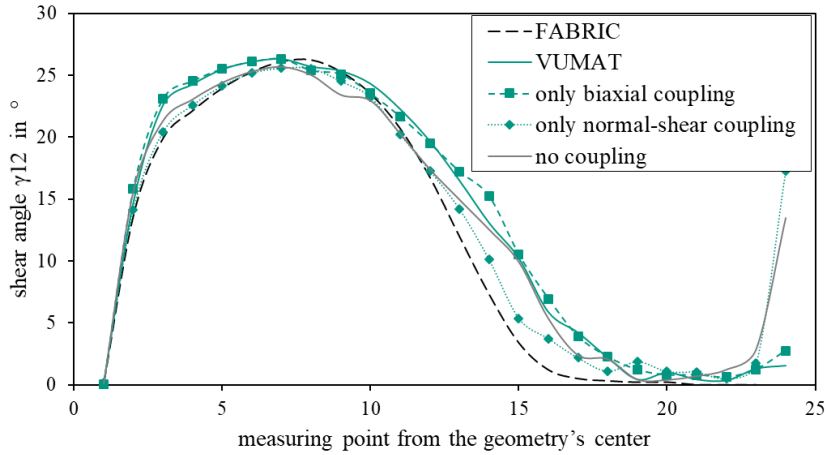

Fig. 7. Shear angle γ_{12} along the dotted line in Fig. 6a within the formed pure woven fabric: Comparison of the FABRIC material model and four different configurations of the new hyperelastic material model.

Summary

Forming simulation at component scale was performed to evaluate the significance of individual coupling effects in constitutive modeling of the fabric plies. For this purpose, a previously proposed invariant-based constitutive model, which includes biaxial and normal-shear coupling for positive and negative strains, was examined at the example of forming simulation to a tetrahedron. To compare the influence of strong and weak forming constraints on the multiaxial coupling effects, a fiber-metal laminate (FML) and a pure fabric laminate were formed to the tetrahedron geometry. Based on the simulation results, it could be shown that biaxial coupling has a significant effect on the forming results, if forming is constrained by adjacent metal layers. In the case of free or almost free draping conditions, this coupling effect is much smaller.

Nevertheless, blank holder forces also cause forming constraints that can partially prevent wrinkling and promote the importance of biaxial strain coupling. The results also revealed that biaxial coupling has a larger influence on the forming results than normal-shear coupling.

Acknowledgement
The support by the German Research Foundation (DFG) for the project HyRTM on FML manufacturing (no. 269244876, HE 6154/4-2) and for the project AMECOMP on textile forming simulation (no. 431354059, KA 4224/6-1) is gratefully acknowledged.

References

[1] P. Bussetta, N. Correia, Numerical forming of continuous fibre reinforced composite material: A review. Composites Part A: Appl. Sci. Manuf. 113 (2018) 12-31. https://doi.org/10.1016/j.compositesa.2018.07.010

[2] P. Boisse, R. Akkerman, P. Carlone, L. Kärger, S.V. Lomov, J.A. Sherwood, Advances in composite forming through 25 years of ESAFORM, Int. J. Mater. Form. 15 (2022) 39. https://doi.org/10.1007/s12289-022-01682-8

[3] L. Kärger, S. Galkin, D. Dörr, C. Poppe, Capabilities of Macroscopic Forming Simulation for Large-Scale Forming Processes of Dry and Impregnated Textiles. Procedia Manuf. 47 (2020) 140-147. https://doi.org/10.1016/j.promfg.2020.04.155

[4] S. Chen, L.T. Harper, A. Endruweit, N.A. Warrior, Formability optimisation of fabric preforms by controlling material draw-in through in-plane constraints. Composites Part A 76 (2015) 10-19. https://doi.org/10.1016/j.compositesa.2015.05.006

[5] L. Kärger, S. Galkin, C. Zimmerling, D. Dörr, J. Linden, A. Oeckerath, K. Wolf: Forming optimisation embedded in a CAE chain to assess the structural performance of composite components. Compo. Struct. 192 (2018) 143-152. https://doi.org/10.1016/j.compstruct.2018.02.041

[6] P. Xue, X. Peng, J. Cao, A non-orthogonal constitutive model for characterizing woven composites, Composites Part A: Appl. Sci. Manuf. 34 (2003) 183-193. https://doi.org/10.1016/S1359-835X(02)00052-0

[7] W. Lee, J. Cao, P. Badel, P. Boisse, Non-orthogonal constitutive model for woven composites incorporating tensile effect on shear behavior, Int. J. Mater. Form. 1 (2008) 891-894. https://doi.org/10.1007/s12289-008-0239-1

[8] P. Badel, E. Vidal-Sallé, P. Boisse, Large deformation analysis of fibrous materials using rate constitutive equations. Comput. Struct. 86 (2008) 1164-1175. https://doi.org/10.1016/j.compstruc.2008.01.009

[9] M.A. Khan, T. Mabrouki, E. Vidal-Sallé, P. Boisse, Numerical and experimental analyses of woven composite reinforcement forming using a hypoelastic behaviour. Application to the double dome benchmark. J. Mater. Process. Technol. 210 (2010) 378-388.

[10] F.J. Schirmaier, D. Dörr, F. Henning, L. Kärger, A macroscopic approach to simulate the forming behaviour of stitched unidirectional non-crimp fabrics. Compos. A 102 (2017) 322-335. http://dx.doi.org/10.1016/j.compositesa.2017.08.009

[11] B. Chen, J. Colmars, N. Naouar, P. Boisse, A hypoelastic stress resultant shell approach for simulations of textile composite reinforcement forming. Composites Part A: Appl. Sci. Manuf. 149 (2021) 106558. https://doi.org/10.1016/j.compositesa.2021.106558

[12] A. Charmetant, J.G. Orliac, E. Vidal-Sallé, P. Boisse, Hyperelastic model for large deformation analyses of 3D interlock composite preforms. Compos. Sci. Technol. 72 (2012) 1352-1360. https://doi.org/10.1016/j.compscitech.2012.05.006

[13] D. Dörr, F. Henning, L. Kärger, Nonlinear hyperviscoelastic modelling of intra-ply deformation behaviour in finite element forming simulation of continuously fibre-reinforced

thermoplastics, Compos. A 109 (2018) 585-596. https://doi.org/10.1016/j.compositesa.2018.03.037
[14] V. N. Khiêm, H. Krieger, M. Itskov, T. Gries, S. E. Stapleton, An averaging based hyperelastic modeling and experimental analysis of non-crimp fabrics. Int J of Solids and Structures 154 (2018) 43-54. https://doi.org/10.1016/j.ijsolstr.2016.12.018
[15] Y. Aimène, E. Vidal-Salle, B. Hagège, F. Sidoroff, P. Boisse, A Hyperelastic Approach for Composite Reinforcement Large Deformation Analysis, Journal of Composite Materials 44 (1) (2010) 5-26. https://doi.org//10.1177/0021998309345348
[16] X. Peng, Z. Guo, T. Du, W.-R. Yu, A simple anisotropic hyperelastic constitutive model for textile fabrics with application to forming simulation, Composites Part B: Engineering 52 (2013) 275-281. https://doi.org/10.1016/j.compositesb.2013.04.014
[17] C. Poppe, D. Dörr, F. Henning, L. Kärger: Experimental and numerical investigation of the shear behaviour of infiltrated woven fabrics, Composites Part A 114 (2018) 327-337. https://doi.org/10.1016/j.compositesa.2018.08.018
[18] Y. Yao, X. Huang, X. Peng, P. Liu, G. Youkun, An anisotropic hyperelastic constitutive model for plain weave fabric considering biaxial tension coupling, Text. Res. J. 89 (2019) 434-444. https://doi.org/10.1177/0040517517748495
[19] Y. Yao, X. Peng, Y. Gong, Influence of tension-shear coupling on draping of plain weave fabrics, J. Mat. Sci. 54 (8) (2019) 6310-6322. https://doi.org/10.1007/s10853-019-03334-w
[20] H.O. Werner, F. Schäfer, F. Henning, L. Kärger, Material Modelling of Fabric Deformation in Forming Simulation of Fiber-Metal Laminates - A Review on Modelling Fabric Coupling Mechanisms, ESAFORM (2021) 2056, Liège, Belgique. https://doi.org/10.25518/esaform21.2056
[21] F. Schäfer, H.O. Werner, F. Henning, L. Kärger, A Hyperelastic Material Model considering Biaxial Coupling of Tension-Compression and Shear for the Forming Simulation of Woven Fabrics, Compos. A: in press (2022) 107323. https://doi.org/10.1016/j.compositesa.2022.107323
[22] H.O. Werner, D. Dörr, F. Henning, L. Kärger, Numerical modeling of a hybrid forming process for three-dimensionally curved fiber-metal laminates, AIP Conference Proceedings 2113 (2019) 020019. https://doi.org/10.1063/1.5112524
[23] H.O. Werner, C. Poppe, F. Henning, L. Kärger, Material Modeling in Forming Simulation of Three-Dimensional Fiber-Metal-Laminates - A Parametric Study, Procedia Manuf. 47 (2020) 154-161. https://doi.org/10.1016/j.promfg.2020.04.160
[24] A. Cherouat, H. Bourouchaki, Numerical Tools for Composite Woven Fabric Preforming, Adv. Mat. Sci. Eng. 2013 (2013) 709495. https://doi.org/10.1155/2013/709495
[25] M. Komeili, Multi-Scale Characterization and Modeling of Shear-Tension Interaction in Woven Fabrics for Composite Forming and Structural Applications, Dissertation, The University of British Columbia, Okanagan, 2014. https://dx.doi.org/10.14288/1.0074335